We are IntechOpen, the world's leading publisher of Open Access books Built by scientists, for scientists

4,800
Open access books available

122,000
International authors and editors

135M
Downloads

Our authors are among the

154
Countries delivered to

TOP 1%
most cited scientists

12.2%
Contributors from top 500 universities

CLARIVATE ANALYTICS BOOK CITATION INDEX INDEXED

WEB OF SCIENCE™

Selection of our books indexed in the Book Citation Index in Web of Science™ Core Collection (BKCI)

Interested in publishing with us?
Contact book.department@intechopen.com

Numbers displayed above are based on latest data collected.
For more information visit www.intechopen.com

2

High-resolution, High-speed 3-D Dynamically Deformable Shape Measurement Using Digital Fringe Projection Techniques

Song Zhang
Iowa State University
USA

1. Introduction

With recent advancements of 3-D geometric shape analysis, acquiring 3-D dynamic scenes in real time becomes increasingly important in enormous fields, such as manufacturing, medical sciences, computer sciences, homeland security, and entertainment, etc.

Over the last decades, 3-D shape measurement techniques have been improving dramatically rapidly. Numerous techniques have been developed including time of flight, stereo vision, structured light, and digital fringe projection. Because of the development of digital display technology, the structured-light-based methods have the potential to be the most important technology for 3-D shape measurement in both scientific research and industrial practices in the long run.

Real-time 3-D shape measurement has recently emerged as a quickly expanding field with the enhancements of computation power of an ordinary personal computer. For real-time 3-D shape measurement, 3-D shapes have to be acquired rapidly, processed quickly, and displayed in real time (Zhang, 2010). In the past few years, a number of technologies have been developed. Among which, the optical method is one of the core techniques. However, due to its fundamentally difficult nature, capturing 3-D dynamic scenes with high quality remains challenging, and even fewer systems are capable of processing 3-D geometry in real time because of the complexity of the problem

Our group has devoted a vast amount of effort in real-time 3-D shape measurement field. Over the past few years, we have been developing technologies using a technique called *digital fringe projection and phase-shifting technique*, a variation of the structured light technique with structured patterns being sinusoidally changing intensity. We have developed a number of algorithms to improve the processing speed, and taken advantage of the most advanced hardware technologies, graphics processing unit (GPU), to increase the speed of 3-D geometry reconstruction and rendering. With these technologies, we have successfully developed a high-resolution, real-time 3-D shape measurement that achieved simultaneous 3-D absolute shape acquisition, reconstruction, and display at a speed of faster than 26 frames / sec with 300K points per frame under an ordinary personal computer (Zhang et al., 2006). Experiments have demonstrated that the system can accurately capture dynamic changing 3-D scenes, such as human facial expressions. The data acquired by such a system have already been applied to

a variety of fields including computer science, medical sciences, and entertainment industry for a variety of purposes.

In this chapter, we will address the most recent advancements in real-time 3-D shape measurement techniques. The principles of different techniques will be explained, and the advantages and limitations of each technology will be discussed. We will especially focus on the high-resolution, real-time 3-D shape measurement techniques using digital fringe projection techniques because of their numerous advantageous features. Finally, we will present some potential applications of real-time 3-D shape measurement, and address some challenges that we are still facing.

We should emphasize that most of the technologies covered in this chapter have already been published in either conference proceedings or journal articles. This chapter, by no means, is an exhaustive survey of real-time 3-D shape measurement technologies. It mainly focuses on the technologies that we have developed over the past few years.

2. Principle of structured light technique

2.1 Introduction

Optical methods to measure 3-D profiles have been extensively used due to their surface noncontact and noninvasive nature. Stereo vision (Dhond & Aggarwal, 1989), which uses two cameras to capture 2-D images from different views, is probably the most well studied of these. This technology simulates human vision, and recovers the depth information via triangulation by knowing the corresponding points between two cameras. Relying on identifying corresponding pairs between two images to recover depth, it is difficult to achieve high accuracy if a surface does not have strong texture variation.

Instead of relying on natural texture, a structured light system uses a projector to actively project predefined structured patterns to assist in correspondence establishment (Salvi et al., 2004). To reach real time, multiple structured patterns are usually switched rapidly so that the number of patterns required to recover one 3-D shape can be captured in a short period of time. Rusinkiewicz et al. (2002) developed a real-time 3-D model acquisition system using a stripe boundary code (Hall-Holt & Rusinkiewicz, 2001). The stripe boundary code is generated by projecting a sequence of binary level structured patterns. Binary-coded structured patterns (only 0's and 1's) are extensively used in a structured light system, because they are (1) simple-it is easy to implement since the coding and decoding algorithms are straightforward, and (2) robust-it is robust to noise because only two intensity levels (0 and 255) are used. Fig. 1(A) shows a binary pattern, and Fig. 1(B) shows its cross section. Here black represents binary level 0, while white represents binary level 1. For a stripe between M and N in Fig. 1(B), all points have the same intensity value, thus cannot be differentiated. Therefore, it is difficult for binary methods to reach pixel-level spatial resolution because the stripe width must be larger than one projector's pixel. Moreover, because it cannot reach pixel level correspondence, it is difficult of this technology to reach very high measurement accuracy.

If more intensity values are used, the spatial resolution will be increased. Coding methods including n-ary (Pan et al., 2004), triangular phase-shifting (Jia et al., 2007), and trapezoidal phase-shifting (Huang et al., 2005) have been developed for higher spatial resolution measurement. As noted by Zhang (2010), all these patterns eventually become sinusoidal if they are blurred properly. The blurring effect often occurs when a camera captures an image out of focus, and all sharp features of an object will be blended together. Therefore, sinusoidal patterns seem to be the natural choice. As shown in Fig. 1(C) and Fig. 1(D), the intensity varies across

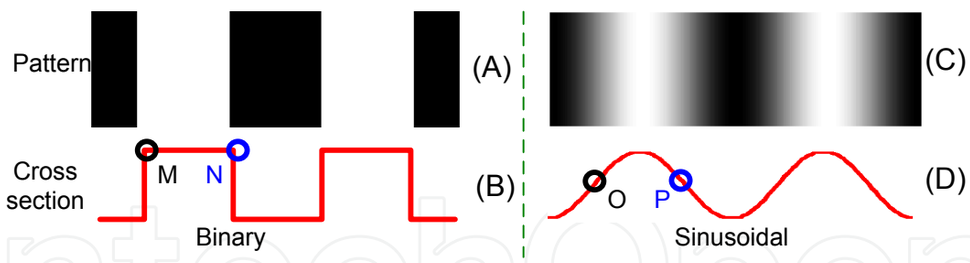

Fig. 1. Comparison between binary and sinusoidal structured pattern. (A) Typical binary structured patterns; (B) Cross section of the binary pattern shown in (A); (C) Typical sinusoidal fringe pattern; (D) Cross section of the sinusoidal patterns as shown in (C).

the image point by point. Therefore, it seems to be feasible to reach pixel level resolution because the intensity values between horizontal neighboring pixels are differentiable. Because the spatial resolution is high, it is possible to achieve high accuracy since the correspondence between the projector and the camera can be determined accurately.

Because using sinusoidal patterns (also known as *fringe patterns*) has the potential to reach pixel-level spatial resolution, it has long been studied in optical metrology where the fringe patterns are generated by laser interference. As noted by Su & Zhang (2009), single B/W fringe image (Guo & Huang, 2009) has been developed to measure dynamic motion of 3-D surfaces using a Fourier method (Takeda & Mutoh, 1983). However, this technique is limited to measuring smooth surfaces. If two fringe patterns are used, the measurement quality is improved (Guo & Huang, 2008). But it is still restricted to measuring surfaces without strong texture and/or geometry variations. To measure generic surfaces, at least three fringe patterns must be used (Schreiber & Bruning, 2007).

3-D shape measurement techniques using color-encoded patterns (Geng, 1996; Harding, 1988; Huang et al., 1999; Pan et al., 2005) have the potential to reach high speed because a structured pattern can be encoded with three fringe patterns. However, the measurement accuracy is affected, to a various degree, by object surface color (Zhang & Huang, 2004). For example, for a blue object, information conveyed by red and green colors will be lost because no signal will be captured. Moreover, the color coupling between red and green, and green and blue will affect the measurement if no filtering is used (Pan et al., 2005).

To avoid the problems induced by color, we developed a 3-D shape measurement system using B/W fringe images (Zhang & Huang, 2006a). By adopting a fast three-step phase-shifting algorithm (Huang & Zhang, 2006), the system achieved simultaneous data acquisition, reconstruction, and display in real time (Zhang et al., 2006). This technique takes advantage of the unique projection mechanism of a single-chip DLP projector: three fringe patterns are encoded into RGB channels of the projector and are switched automatically and naturally. By this means, we achieved 3-D surface measurement at 60 Hz with more than 300K points per frame (Zhang & Yau, 2007). We will discuss the details of this technology next.

2.2 Digital fringe projection system setup

A digital fringe projection system is very simple: it contains a projector to project fringe patterns, a camera to capture the fringe patterns, and the computer software to analyze the fringe images to recover the 3-D shape. Fig. 2 shows the schematic diagram of a 3-D imaging system

based on a digital fringe projection technique. A projector projects vertically (varying horizontally) straight fringe stripes (phase lines) onto the object. The object surface distorts the fringe images from straight phase lines to curved ones. A camera images the distorted fringe images from another viewing angle. If the corresponding point between the camera pixel (A) and the projector pixel (C) is identified, depth (z) can be recovered through triangulation (ΔABC).

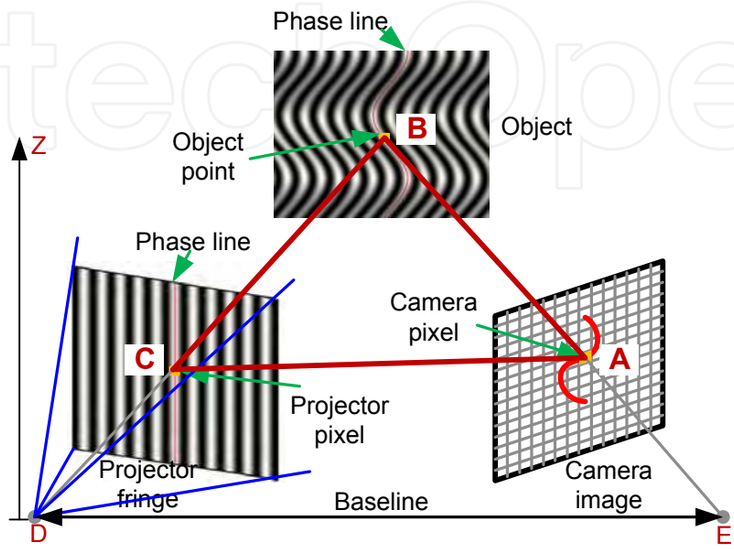

Fig. 2. Schematic diagram of a 3-D shape measurement system with a digital fringe projection technique. A fringe pattern is projected onto an object, the object surface geometry distorts and reflects the fringe pattern, and a camera, viewing from another angle captures the reflected fringe pattern. Because the projector and the camera form a triangular relationship, if the correspondence between the camera and the projector is known, 3-D information can be obtained through triangulation.

2.3 Phase-shifting algorithm

To establish the correspondence between the captured images and the projected images, the structured light system based on binary methods uses *codewords*. The codeword, a unique value, is formed by a sequence of stripes composed of 0's (purely black) or 1's (purely white) and can be determined from captured images. As explained previously, a method using binary structured patterns cannot reach pixel-level resolution spatially, while a technique based on sinusoidal fringe patterns has the potential to do so.

We used a digital fringe projection and phase-shifting method to reach higher spatial and temporal resolution for 3-D shape measurement. For this method, the codeword is determined by the phase that is calculated from the fringe images. To increase measurement speed, the minimum number of fringe images (three) is used. Their intensities can be written as

$$I_1(x,y) = I'(x,y) + I''(x,y)\cos[\phi(x,y) - 2\pi/3], \quad (1)$$

$$I_2(x,y) = I'(x,y) + I''(x,y)\cos[\phi(x,y)], \quad (2)$$

$$I_3(x,y) = I'(x,y) + I''(x,y)\cos[\phi(x,y) + 2\pi/3]. \quad (3)$$

Where $I'(x,y)$ is the average intensity, $I''(x,y)$ the intensity modulation, $\phi(x,y)$ the phase to be solved for. Solving Eqs. (1)–(3) simultaneously, we will obtain the phase

$$\phi(x,y) = \tan^{-1}\left[\frac{\sqrt{3}(I_1 - I_3)}{2I_2 - I_1 - I_3}\right], \tag{4}$$

Equation (4) indicates that the phase ranges from -π to +π with 2π discontinuities.
From Eqs. (1)–(3), we can also obtain a texture image,

$$\begin{aligned} I_t(x,y) &= I'(x,y) + I''(x,y) \\ &= \frac{(I_1 + I_2 + I_3)}{3} + \frac{\sqrt{3(I_1 - I_3)^2 + (2I_2 - I_1 - I_3)^2}}{3}. \end{aligned} \tag{5}$$

The texture image is the photograph of the object without fringe stripes. Although irrelevant to optical metrology, texture image plays a key role in many fields for shape analysis to industrial inspection, because it provides vital information of the object. In computer graphics, texture image is mostly used for enhancing visual effect by a technique called texture mapping.
In addition, we can also obtain intensity modulation

$$\gamma(x,y) = \frac{I''(x,y)}{I'(x,y)} = \frac{\sqrt{3(I_1 - I_3)^2 + (2I_2 - I_1 - I_3)^2}}{I_1 + I_2 + I_3} \tag{6}$$

Intensity modulation indicates the fringe quality, or the contrast of the fringe images, with 1 being the best. It is usually used to separate the background and the foreground, and sometime used to analyze the phase.

2.4 Phase unwrapping technique

To obtain a continuous phase map from the wrapped phase map determined by Eq. (4), a conventional method is to adopt a phase unwrapping algorithm. The phase unwrapping is essentially to detect 2π discontinuities based on its neighboring phase values and remove them by adding or subtracting multiples of 2π. In other words, the phase unwrapping is to

$$\Phi(x,y) = \phi(x,y) + 2k\pi. \tag{7}$$

Here, k is an integer.
Robust phase unwrapping is usually very time-consuming because it involves a lot computation as well as iterations. The processing time ranges from seconds to minutes, and even to hours (Ghiglia & Pritt, 1998). To improve the robustness of the phase unwrapping step, numerous algorithms have been developed including the branch-cut algorithms (Huntley, 1989), the discontinuity minimization algorithm (Flynn, 1997), the L^p-norm algorithm (Ghiglia & Romero, 1996), and the region growing algorithm (Baldi, 2003). However, they are generally too slow for real-time applications. Some fast phase unwrapping algorithms, such as a flood filling algorithm, can unwrap the phase rapidly (Zhang & Huang, 2006a). However, they are usually very sensitive to the noise of the phase map. To solve the dilemma, we developed a multilevel quality-guided phase unwrapping algorithm (Zhang et al., 2007), which will be discussed in Section 3.2

2.5 Absolute phase retrieval

The phase in Eq. (7), is often regarded as *relative phase*, because it is relative to one point on the phase map that is usually determined from the phase unwrapping stage. *Absolute phase* is the phase value that is relative to the pre-defined phase. In a digital fringe projection and phase-shifting system, the phase obtained from the computer generated fringe images can be regarded as the pre-defined phase values, thus the absolute phase. To obtain absolute phase from the captured fringe images, at least one point within one connected patch must have the known phase value. A marker, such as a point, a line, or any other vivid features can be used as references to convert the relative phase to absolute one. The marker is projected by the projector and captured by the camera. The software algorithm is then used to identify the marker points. Because the phase on the marker point is pre-defined theoretically, the relative phase needs to be shifted to ensure that the marker point phase is the same as that of the pre-defined one. Assume that the reference point on the computer generated fringe images has the absolute phase of 0, and the relative phase ϕ_0 that is calculated from the camera captured images, the relative phase map can be converted to absolute one by the following equation

$$\phi_a(x,y) = \phi(x,y) - \phi_0. \tag{8}$$

2.6 Structured light system calibration

3-D information is carried on by the phase, from which the 3-D coordinates of the object can be recovered. Conventionally, a reference plane is utilized, and any measurement is relative to it (Huang et al., 2002). For smaller range measurement, the depth information (z coordinate) is approximately proportional to the phase difference between the measured phase value and the reference phase value. However, the drawbacks of using a reference plane are:

1. *Approximation*. Accurate coordinates for each point is very difficult to obtain.
2. *Small range measurement*. The depth range must be very small relative to its distance from the hardware system. Otherwise, the approximation error is significant.
3. *Inaccurate x and y coordinates*. This approach in general only obtains the depth z information, while x and y coordinates are ignored.

To circumvent the approximation errors, the system has be to calibrated. One of the key to calibrate the structured light system is to calibrate a camera accurately. The camera calibration is essentially to find the intrinsic parameters (e.g. focal length, principle point), and extrinsic parameter, the transformation between the (x,y,z) coordinates in a world coordinate system (x^w,y^w,z^w), and that in the camera coordinate system. Among the models created, Zhang's calibration model is most widely adopted in computer vision field (Zhang, 2000). In this model, the camera is treated as a pinhole system as shown in Fig. 3, and the intrinsic parameter is represented as,

$$A = \begin{bmatrix} \alpha & \kappa & u_0 \\ 0 & \beta & v_0 \\ 0 & 0 & 1 \end{bmatrix}. \tag{9}$$

Where (u_0,v_0) is the coordinate of the principle point, the intersection between the optical axis and the image sensor, α and β are the focal lengths along u and v axes of the image plane, and κ is the parameter that represents the skewness of uv coordinate system.
And extrinsic parameters can be described as,

$$[R,t] = \begin{bmatrix} r_{11} & r_{12} & r_{13} & t_x \\ r_{21} & r_{22} & r_{23} & t_y \\ r_{31} & r_{32} & r_{33} & t_z \end{bmatrix}. \tag{10}$$

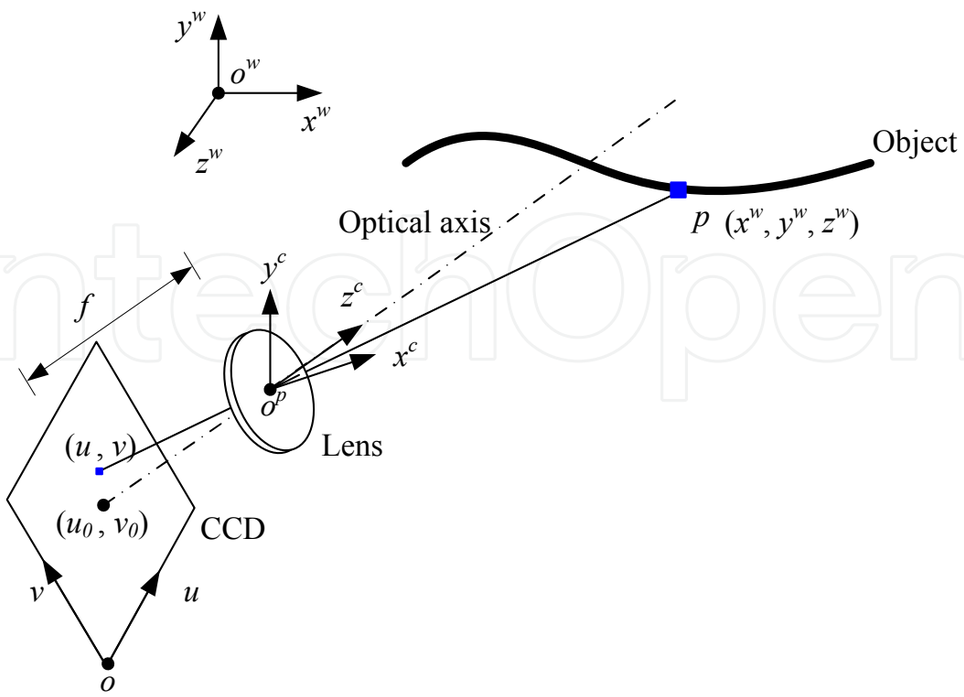

Fig. 3. Pinhole camera model. The camera model is to describe that an arbitrary point in 3-D space under its own coordinate system is transformed to the camera lens coordinate system, and finally 3-D coordinates in lens coordinate system are projected onto a 2-D imaging space.

Here R is the rotation 3×3 matrix, and t is a 3×1 translation vector.
Fig. 3 shows the typical diagram of a pinhole camera model, where p is an arbitrary point with coordinates (x^w, y^w, z^w) in the world coordinate system $(0^w; x^w, y^w, z^w)$, and (x^c, y^c, z^c) in the camera coordinate system $(0^c; x^c, y^c, z^c)$. If p is projected onto the image plane, the relationship between the world coordinates and the image coordinates can be represented as

$$sI = A[\ R, \quad t\ ]X^w, \tag{11}$$

Where $I = [u, v, 1]^T$ is the homogeneous coordinate of the image point in the image plane, $X^w = [x^w, y^w, z^w, 1]^T$ the homogeneous world coordinate for that point, and s a scaling factor. The above equation describes a linear camera model, the nonlinear effects can be compensated for by adopting a nonlinear model.
Unlike a camera-camera (stereo) system, a structured light system calibration involves projector calibration that is usually not simple because it cannot capture images like a regular camera. Numerous techniques have been proposed (Cuevas et al., 1999; Hu et al., 2003). However, most of these techniques are time-consuming and very difficult to achieve high accuracy. Legarda-Sáenz et al. (2004) proposed a method that uses absolute phase to find the marker centers of the calibration board for the projector by projecting a sequence of fringe patterns. Through optimization, this method performed well in terms of accuracy. However, it requires the use of the calibrated camera to calibrate the projector, thus the calibration errors of the camera will bring into the projector calibration, which is not desirable.

Zhang & Huang (2006b) proposed a new structured light system calibration method. In this method, the fringe images are used as a tool to establish the mapping between the camera pixel and the projector pixel so that the projector can “capture" images like a camera. By this means, the structured light system calibration becomes a well studied stereo system calibration. Since the projector and the camera are calibrated independently and simultaneously, the calibration accuracy is significantly improved, and the calibration speed is drastically increased. Fig. 4 shows a typical checkerboard image pair captured by the camera, and the projector image converted by the mapping method. It clearly shows that the projector checkerboard image is well captured. By capturing a number of checkerboard image pairs and applying the software algorithm developed by Bouguet (http://www.vision.caltech.edu/bouguetj/calib_doc), both the camera and the projector are calibrated at the same time.

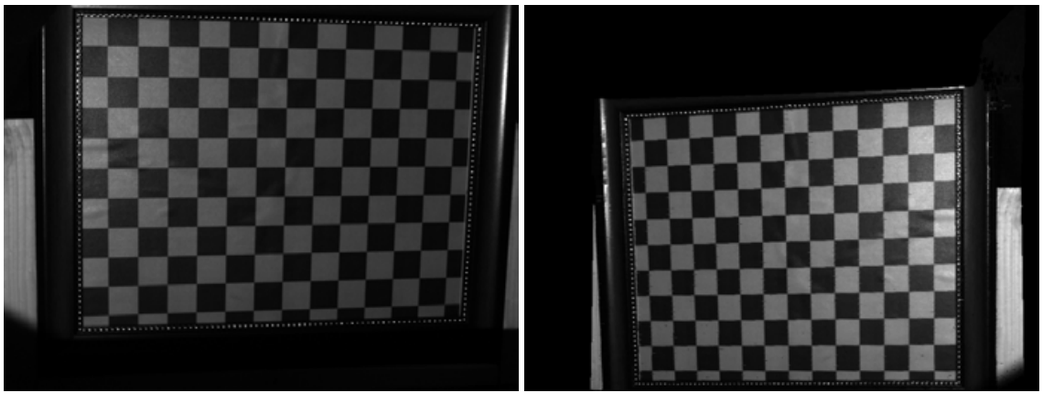

(a) (b)

Fig. 4. Checkerboard image pair by using the proposed technique by Zhang and Huang (Zhang & Huang, 2006b). (a) The checkerboard image captured by the camera; (b) The mapped checkerboard image for the projector, which is regarded as the checkerboard image captured by the projector.

Following the work by Zhang & Huang (2006b), a number of calibration approaches have been developed (Gao et al., 2008; Huang & Han, 2006; Li et al., 2008; Yang et al., 2008). All these techniques are essentially the same: to establish the one-to-one mapping between the projector and the camera. Our recent work showed that the checker size of the checkerboard plays a key role (Lohry et al., 2009), and a certain range of checker size will give better calibration accuracy. This study provides some guidelines for selecting the checker size for precise system calibration. Once the system is calibrated, the *xyz* coordinates can be computed from the *absolute* phase, which will be addressed in the next subsection.

2.7 3-D coordinate calculation from the absolute phase

Once the absolute phase map is obtained, the relationship between the camera sensor and projector sensor will be established as a one-to-many mapping, i.e., one point on the camera sensor corresponds to one line on the projector sensor with the same absolute phase value. This relationship provides a constraint for the correspondence of a camera-projector system. If the camera and the projector are calibrated in the same world coordinate system, and the

linear calibration model is used for both the camera and the projector, Eq. (11) can be re-written as

$$s^c I^c = A^c [\ R^c, \quad t^c\ ] X^w. \tag{12}$$

Here, s^c is the scaling factor for the camera, I^c the homogeneous camera image coordinates, A^c the intrinsic parameters for the camera, and $[R^c, t^c]$ the extrinsic parameter matrix for the camera.

Similarly, the relationship between the projector image point and the object point in the world coordinate system can be written as

$$s^p I^p = A^p [\ R^p, \quad t^p\ ] X^w. \tag{13}$$

Here s^p is the scaling factor for the projector, I^p the homogeneous projector image coordinates, A^p the intrinsic parameters for the projector, $[R^p, t^p]$ the extrinsic parameter matrix for the projector.

In addition, because absolute phase is known, each point on the camera corresponds to one line with the same absolute phase on the projected fringe image (Zhang & Huang, 2006b). That is, assume the fringe stripe is along v direction, we can establish a relationship between the captured fringe image and the projected fringe image,

$$\phi_a(u^c, v^c) = \phi_a(u^p). \tag{14}$$

In Equations (12)-(14), there are seven unknowns $(x^w, y^w, z^w), s^p, s^p, u^p$, and v^p, and seven equations, the world coordinates (x^w, y^w, z^w) can be uniquely solved for.

2.8 Example of measurement

Fig. 5 shows an example of 3-D shape measurement using a three-step phase-shifting method. Fig. 5(a)-5(c) shows three phase-shifted fringe images with $2\pi/3$ phase shift. Fig. 5(d) shows the phase map after applying Eq. (4) to these fringe images, it clearly shows phase discontinuities. Applying the phase unwrapping algorithm discussed in Reference (Zhang et al., 2007), this wrapped phase map can be unwrapped to get a continuous phase map as shown in Fig. 5(e). The unwrapped phase map is then converted to 3-D shape by applying method introduced in Section 2.7. The 3-D shape can be rendered by OpenGL, as shown in Figs. 5(f)-5(g). At the same time, by averaging these three fringe images, a texture image can be obtained, which can be mapped onto the 3-D shape to for better visual effect, as seen in Fig. 5(h).

3. Real-time 3-D Shape Measurement Techniques

3.1 Hardware implementation of phase-shifting technique for real-time data acquisition

From Section 2, we know that, for a three-step phase-shifting algorithm, only three images are required to reconstruct one 3-D shape. This, therefore, permits the possibility of encoding them into a single color image. As explained in Section 2, using color fringe pattern is not desirable for 3-D shape measurement because of the problems caused by color. To avoid this problem, we developed a real-time 3-D shape measurement system based on a single-chip DLP projection and white light technique (Zhang & Huang, 2006a).

Fig. 6 shows the system layout. Three phase-shifted fringe images are encoded with the RGB color channel of a color fringe image generated by the computer. The color image is then sent to the single-chip DLP projector that switches three-color channels sequentially onto the object; a high-speed CCD camera, synchronized with the projector, is to capture three phase-shifted fringe images at high speed. Any three fringe images can be used to reconstruct one

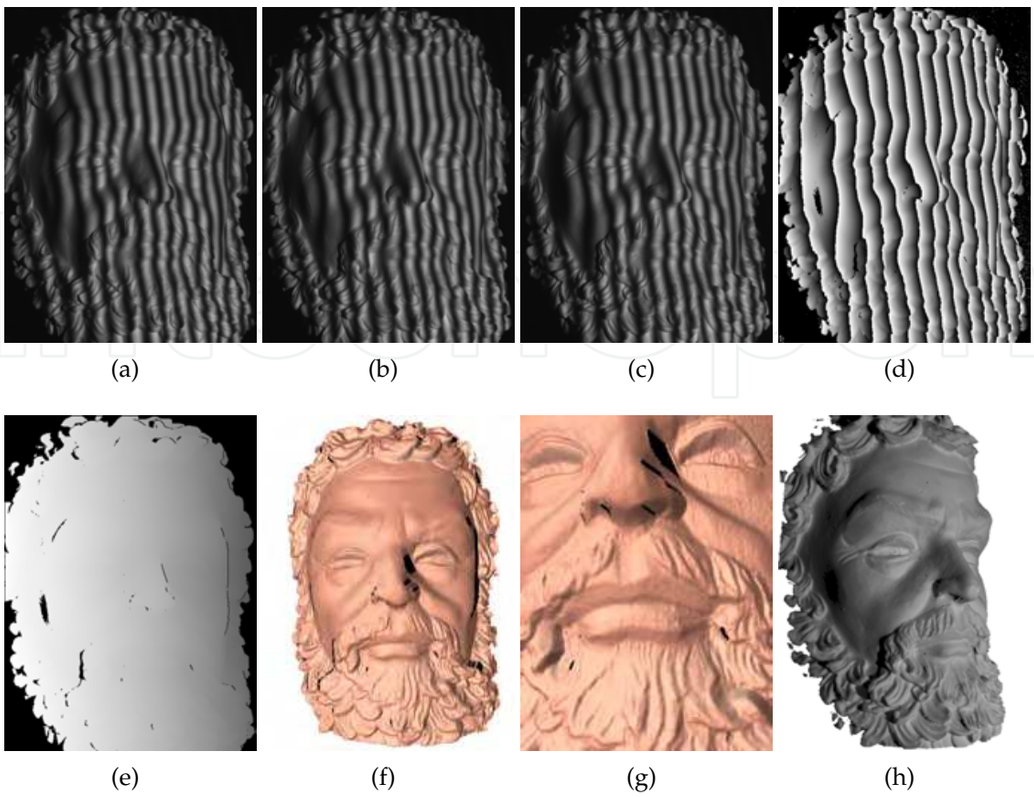

Fig. 5. . Example of 3-D shape measurement using a three-step phase-shifting method. (a) $I_1(-2\pi/3)$; (b) $I_2(0)$; (c) $I_3(2\pi/3)$; (d) Wrapped phase map; (e) Unwrapped phase map; (f) 3-D shape rendered in shaded mode; (g) Zoom in view; (h) 3-D shape rendered with texture mapping.

3-D shape through phase wrapping and unwrapping. Moreover, by averaging these three fringe images, a texture image (without fringe stripes) can be generated. It can be used for texture mapping purposed to enhance certain view effect.

The projector projects a monochrome fringe image for each of the RGB channels sequentially; the color is a result of a color wheel placed in front of a projection lens. Each “frame" of the projected image is actually three separate images. By removing the color wheel and placing each fringe image in a separate channel, the projector can produce three fringe images at 120 fps (360 individual fps). Therefore, if three fringe images are sufficient to recover one 3-D shape, the 3-D measurement speed is up to 120 Hz. However, due to the speed limit of the camera used, it takes two projection cycles to capture three fringe images, thus the measurement speed is 60 Hz. Fig. 7 shows the timing chart for the real-time 3-D shape measurement system.

3.2 Fast phase-shifting algorithm

The hardware system described in previous subsection can acquire fringe images at 180 Hz. However, the processing speed needs to keep up with the data acquisition for real-time 3-D shape measurement. The first challenge is to increase the processing speed of the phase

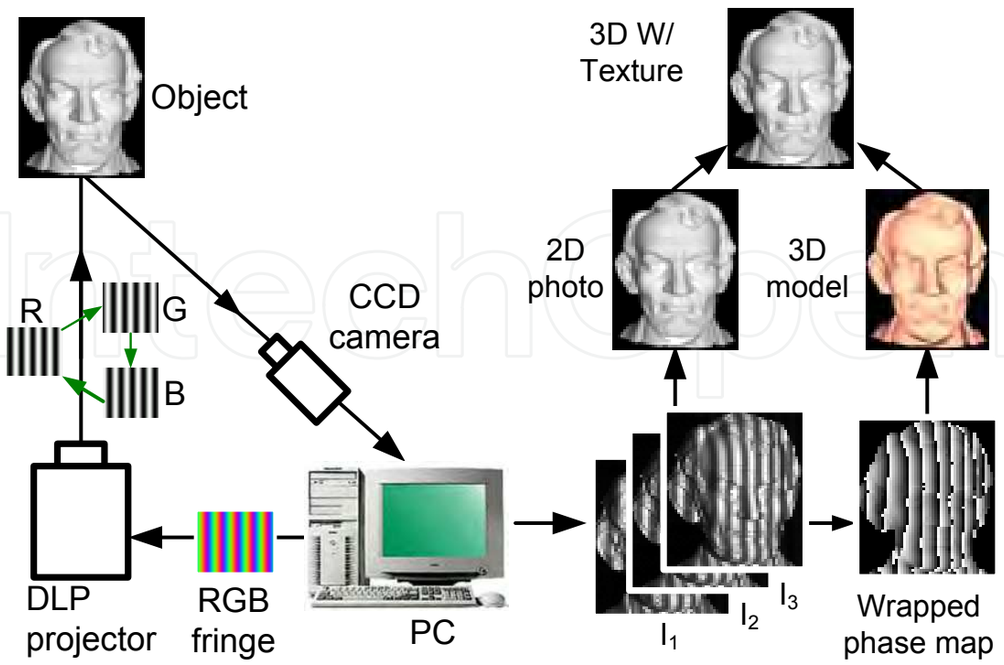

Fig. 6. Real-time 3-D shape measurement system layout. The computer generated color encoded fringe image is sent to a single-chip DLP projector that projects three color channels sequentially and repeatedly in grayscale onto the object. The camera, precisely synchronized with projector, is used to capture three individual channels separately and quickly. By applying the three-step phase-shifting algorithm to three fringe images, the 3-D geometry can be recovered. Averaging three fringe images will result in a texture image that can be further mapped onto 3-D shape to enhance certain visual effect.

wrapping. Experiments found that calculating the phase using Eq. (4) is relatively slow for the purpose of real-time 3-D shape measurement. To improve the processing speed, Huang et al. (2005) developed a new algorithm named trapezoidal phase-shifting algorithm. The advantage of this algorithm is that it processes the phase by intensity ratio instead of arctangent function, thus significantly improves the processing speed (more than 4 times faster). However, the drawback of this algorithm is that the defocusing of the system will introduce error, albeit to a less degree. This is certainly not desirable. Because the sinusoidal fringe patterns are not very sensitive to defocusing problems, we applied the same processing algorithm to sinusoidal fringe, the purpose is to maintain the advantage of processing speed while alleviate the defocusing problem, this new algorithm is called fast three-step phase-shifting algorithm (Huang & Zhang, 2006).

Fig. 8 illustrates this fast three-step phase-shifting algorithm. Instead of calculating phase using an arctangent function, the phase is approximated by intensity ratio

$$r(x,y) = \frac{I_{med}(x,y) - I_{min}(x,y)}{I_{max}(x,y) - I_{min}(x,y)}. \tag{15}$$

Here I_{max}, I_{med}, I_{min} respectively refer to the maximum, median, and minimum intensity value for three fringe images for the same point. The intensity ratio gives values ranging from [0,

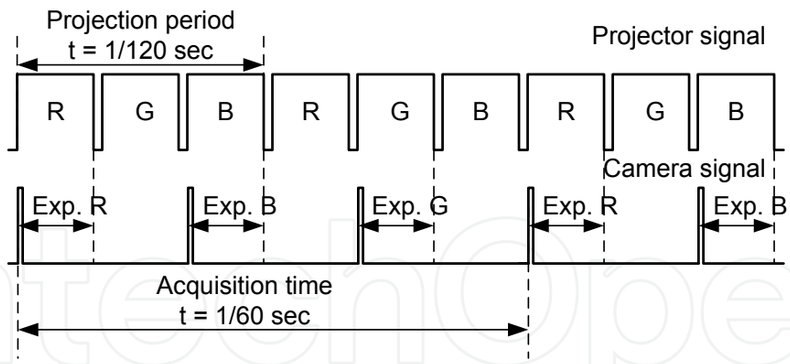

Fig. 7. System timing chart.

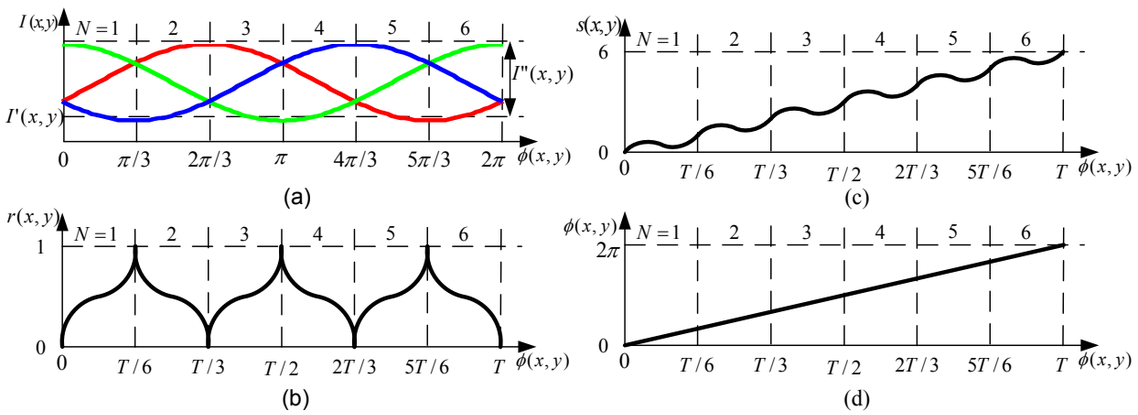

Fig. 8. Schematic illustration for fast three-step phase-shifting algorithm. (a) One period of fringe is uniformly divided into six regions; (b) The intensity ratio for one period of fringe; (c) After slope map after removing the sawtooth shape of the intensity ratio map; (d) The phase after compensate for the approximation error and scaled to its original phase value.

1] periodically within one period of the fringe pattern. Fig. 8(a) shows that one period of the fringe pattern is uniformly divided into six regions. It is interesting to know that the region number N can be uniquely identified by comparing the intensity values of three fringe images point by point. For example, if red is the largest, and blue is the smallest, the point belongs to region $N = 1$. Once the region number is identified, the sawtooth shape intensity ratio in Fig. 8(b) can be converted to its slope shape in Fig. 8(c) by using the following equation

$$s(x,y) = 2 \times Floor\left(\frac{N}{2}\right) + (-1)^{N-1} r(x,y). \tag{16}$$

Here the operator $Floor()$ is used to truncate the floating point data to keep the integer part only. The phase can then be computed by

$$\phi(x,y) = 2\pi \times s(x,y). \tag{17}$$

Because the phase is calculated by a linear approximation, the residual error appears. Since the phase error is fixed in the phase domain, it can be compensated for by using a look-up-table (LUT). After the phase error compensation, the phase will be a linear slope as illustrated

in Fig. 8(d). Experiments found that by using this fast three-step phase-shifting algorithm, the 3-D shape measurement speed is approximately 3.4 times faster.

Phase unwrapping step usually is the most timing-consuming part for 3-D shape measurement based on fringe analysis. Therefore, developing an efficient and robust phase unwrapping algorithm is vital to the success of real-time 3-D shape measurement. Traditional phase unwrapping algorithms are either less robust (such as flood-fill methods) or time consuming (such quality-guided methods). We have developed a multi-level quality-guided phase unwrapping algorithm (Zhang et al., 2007). It is a good trade-off between robustness and efficiency: the processing speed of the quality-guided phase unwrapping algorithm is augmented by the robustness of the scanline algorithm. The quality map was generated from the gradient of the phase map, and then quantized into multi-levels. Within each level point, the fast scanline algorithm was applied. For a three-level algorithm, it only takes approximately 18.3 ms for a 640×480 resolution image, and it could correctly reconstruct more than 99% of human facial data.

By adopting the proposed fast three-step phase-shifting algorithm and the rapid phase unwrapping algorithm, the continuous phase map can be reconstructed in a timely manner. In order to do 3-D coordinates calculations, it involves very intensive matrix operations including matrix inversion, it was found impossible to perform all the calculations in real-time with an ordinary dual CPU workstation. To resolve this problem, new computational hardware technology, graphics processing unit (GPU), was explored, which will be introduced in the next subsection.

3.3 Real-time 3-D coordinates calculation and visualization using GPU

Computing 3-D coordinates from the phase is computationally intensive, which is very challenging for a single computer CPU to realize in real-time. However, because the coordinate calculations are point by point matrix operations, this can be performed efficiently by a GPU. A GPU is a dedicated graphics rendering device for a personal computer or game console. Modern GPUs are very efficient at manipulating and displaying computer graphics, and their highly parallel structure makes them more effective than typical CPUs for parallel computation algorithms. Since there are no memory hierarchies or data dependencies in the streaming model, the pipeline maximizes throughput without being stalled. Therefore, whenever the GPU is consistently fed by input data, performance is boosted, leading to an extraordinarily scalable architecture (Ujaldon & Saltz, 2005). By utilizing this streaming processing model, modern GPUs outperform their CPU counterparts in some general-purpose applications, and the difference is expected to increase in the future (Khailany et al., 2003).

Fig. 9 shows the GPU pipeline. CPU sends the vertex data including the vertex position coordinates and vertex normal to GPU which generates the lighting of each vertex, creates the polygons and rasterizes the pixels, then output the rasterized image to the display screen. Modern GPUs allow user specified code to execute within both the vertex and pixel sections of the pipeline which are called vertex shader and pixel shader, respectively. Vertex shaders are applied for each vertex and run on a programmable vertex processor. Vertex shaders takes vertex coordinates, color, and normal information from the CPU.The vertex data is streamed into the GPU where the polygon vertices are processed and assembled based on the order of the incoming data. The GPU handles the transfer of streaming data to parallel computation automatically. Although the clock rate of a GPU might be significantly slower than that of a CPU, it has multiple vertex processors acting in parallel, therefore, the throughput of the GPU

can exceed that of the CPU. As GPUs increase in complexity, the number of vertex processors increase, leading to great performance improvements.

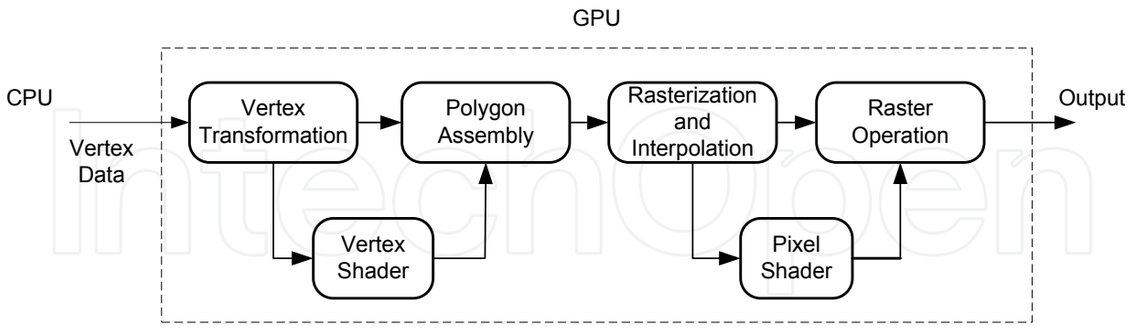

Fig. 9. GPU pipeline. Vertex data including vertex coordinates and vertex normal are sent to the GPU. GPU generates the lighting of each vertex, creates the polygons and rasterizes the pixels, then output the rasterized image to the display screen.

By taking advantage of the processing power of the GPU, 3-D coordinate calculations can be performed in real time with an ordinary personal computer with a decent NVidia graphics card (Zhang et al., 2006). Moreover, because 3-D shape data are already on the graphics card, they can be rendered immediately without any lag. Therefore, by this means, real-time 3-D geometry visualization can also be realized in real time simultaneously. Besides, because only the phase data, instead of 3-D coordinates plus surface normal, are transmitted to graphics card for visualization, this technique reduces the data transmission load on the graphics card significantly, (approximately six times smaller). In short, by utilizing the processing power of GPU for 3-D coordinates calculations, real-time 3-D geometry reconstruction and visualization can be performed rapidly and in real time.

3.4 Experimental results

Fig. 10 shows one of the hardware systems that we developed. The hardware system is composed of a DLP projector (PLUS U5-632h), a high-speed CCD camera (Pulnix TM-6740CL) and a timing generation circuit. The projector has an image resolution of 1024×768, and the focal length of f = 18.4-22.1 mm. The camera resolution is 640×480, and the lens used is a Fujinon HF16HA-1B f = 16 mm lens. The maximum data speed for this camera is 200 frames per second (fps). The maximum data acquisition speed achieved for this 3-D shape measurement system is 60 fps.

With this speed, dynamically deformable 3-D objects, such as human facial expressions, can be effectively captured. Fig. 11 shows some typical measurement results of a human facial expression. The experimental results demonstrate that the details of human facial expression can be effectively captured. At the same time, the motion process of the expression is precisely acquired.

By adopting the fast three-step phase-shifting algorithm introduced in Reference (Huang & Zhang, 2006), the fast phase-unwrapping algorithm explained in Reference (Zhang et al., 2007), and the GPU processing detailed in Reference (Zhang et al., 2006), we achieved simultaneous data acquisition, reconstruction, and display at approximately 26 Hz. The computer used for this test contained Dual Pentium 4 3.2 GHz CPUs, and an Nvidia Quadro FX 3450 GPU. Fig. 12 shows a measurement result. The right shows the real subject and

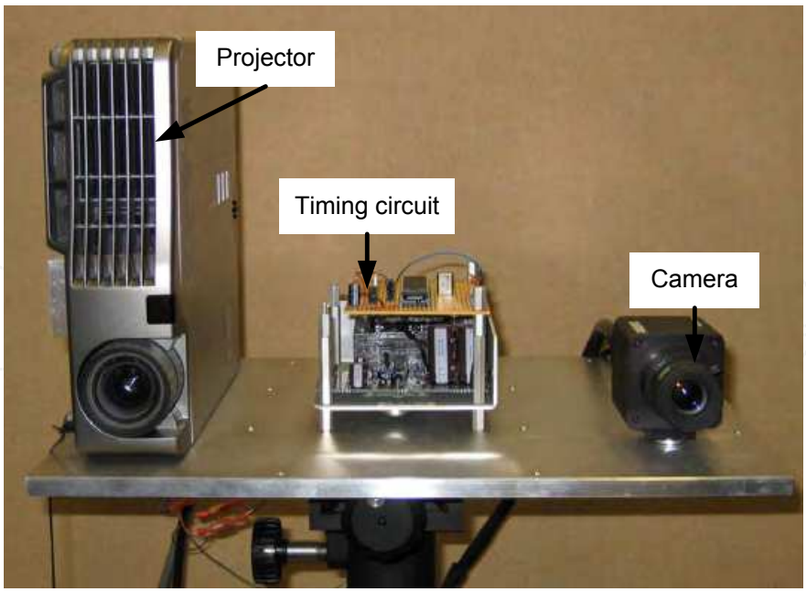

Fig. 10. Photograph of the real-time 3-D shape measurement system. It comprises a DLP projector, a high-speed CCD camera, and a timing signal generator that is used to synchronize the projector with the camera. The size of the system is approximately 24″ × 14″ × 14″.

the left shows the 3-D model reconstructed and displayed on the computer monitor instantaneously. It clearly shows that the technology we developed can perform high-resolution, real-time 3-D shape measurement. More measurement results and videos are available at `http://www.vrac.iastate.edu/~song`.

4. Potential Applications

Bridging between real-time 3-D shape measurement technology and other fields is essential to driving the technology advancement, and to propelling its deployment. We have made significant effort to explore its potential applications. We have successfully applied this technology to a variety of fields. This section will discuss some applications including those we have explored.

4.1 Medical sciences

Facial paralysis is a common problem in the United States, with an estimated 127,000 persons having this permanent problem annually (Bleicher et al., 1996). High-speed 3-D geometry sensing technology could assist with diagnosis; several researchers have attempted to develop objective measures of facial functions (Frey et al., 1999; Linstrom, 2002; Stewart et al., 1999; Tomat & Manktelow, 2005), but none of which have been adapted for clinical use due to the generally cumbersome, nonautomated modes of recording and analysis (Hadlock et al., 2006). The high-speed 3-D shape measurement technology fills this gap and has the potential to diagnose facial paralysis objectively and automatically (Hadlock & Cheney, 2008). A pilot study has demonstrated its feasibility and its great potential for improving clinical practices (Mehta et al., 2008).

Fig. 11. Measurement result of human facial expressions. The data is acquired at 60 Hz, the camera resolution is 640 × 480.

4.2 3-D computer graphics

3-D computer facial animation, one of the primary areas of 3-D computer graphics, has caused considerable scientific, technological, and artistic interest. As noted by Bowyer et al. (Bowyer et al., 2006), one of the grand challenges in computer analysis of human facial expressions is acquiring natural facial expressions with high fidelity. Due to the difficulty of capturing high-quality 3-D facial expression data, conventional techniques (Blanz et al., 2003; Guenter et al., 1998; Kalberer & Gool, 2002) usually require a considerable amount of manual inputs (Wang et al., 2004). The high-speed 3-D shape measurement technology that we developed benefits this field by providing photorealistic 3-D dynamic facial expression data that allows computer scientists to develop automatic approaches for 3-D facial animation. We have been collaborating with computer scientists in this area and have published several papers (Huang et al., 2004; Wang et al., 2008; 2004).

4.3 Infrastructure health monitoring

Finding the dynamic response of infrastructures under loading/unloading will enhance the understanding of their health conditions. Strain gauges are often used for infrastructure health monitoring and have been found successful. However, because this technique usually measures a point (or small area) per sensor, it is difficult to obtain a large-area response unless a sensor network is used. Area 3-D sensors such as scanning laser vibrometers provide more information (Staszewski, 2007), but because of their low temporal resolution, they are difficult to apply for high-frequency study. Kim et al. (2007) noted that using a kilo Hz sensor is sufficient to monitor high-frequency phenomena. Thus, the high-speed 3-D shape measurement technique may be applied to this field.

4.4 Biometrics for homeland security

3-D facial recognition is a modality of the facial recognition method in which the 3-D shape of a human face is used. It has been demonstrated that 3-D facial recognition methods can achieve significantly better accuracy than their 2-D counterparts, rivaling fingerprint recognition (Bronstein et al., 2005; Heseltine et al., 2008; Kakadiaris et al., 2007; Queirolo et al., 2009). By measuring the geometry of rigid features, 3-D facial recognition avoids such pitfalls of 2-D

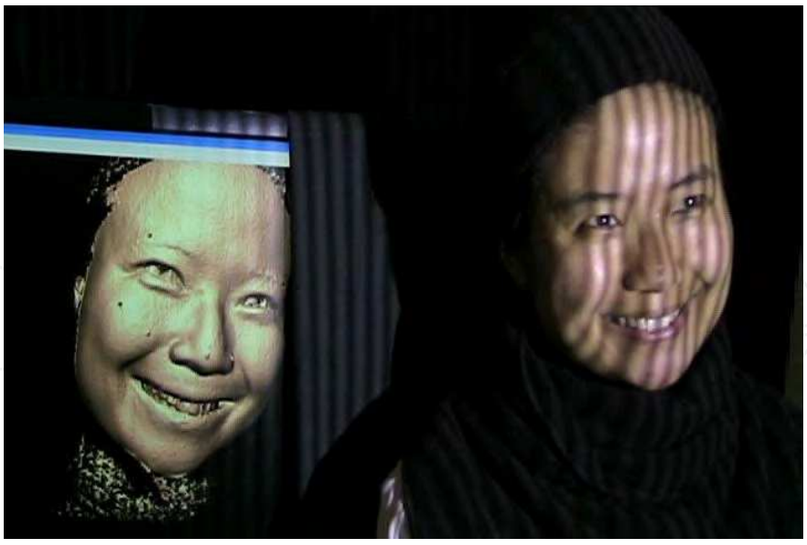

Fig. 12. Simultaneous 3-D data acquisition, reconstruction and display in real-time. The right shows human subject, while the left shows the 3-D reconstructed and displayed results on the computer screen. The data is acquired at 60 Hz and visualized at approximately 26 Hz.

peers as change in lighting, different facial expressions, make-up, and head orientation. Another approach is to use a 3-D model to improve the accuracy of the traditional image-based recognition by transforming the head into a known view. The major technological limitation of 3-D facial recognition methods is the rapid acquisition of 3-D models. With the technology we developed, high-quality 3-D faces can be captured even when the subject is moving. The high-quality scientific data allows for developing software algorithms to reach 100% identification rate.

4.5 Manufacturing and quality control

Measuring the dimensions of mechanical parts on the production line for quality control is one of the goals in the manufacturing industry. Technologies relying on coordinate measuring machines or laser range scanning are usually very slow and thus cannot be performed for all parts. Samples are usually taken and measured to assure the quality of the product. A high-speed dimension measurement device that allows for 100% product quality assurance will significantly benefit this industry.

5. Challenges

High-resolution, real-time 3-D shape measurement has already emerged as an important means for numerous applications. The technology has advanced rapidly recently. However, for the real-time 3-D shape measurement technology that was discussed in this chapter, there some major limitations:

1. *Single object measurement*. The basic assumptions for correct phase unwrapping and 3-D reconstruction require the measurement points to be smoothly connected (Zhang et al., 2007). Thus, it is impossible to measure multiple objects simultaneously.
2. *"Smooth" surfaces measurement*. The success of a phase unwrapping algorithm hinges on the assumption that the phase difference between neighboring pixels is less than

π . Therefore, any step height causing a phase change beyond π cannot be correctly recovered.

3. *Maximum speed of 120 Hz*. Because sinusoidal fringe images are utilized, at least an 8-bit depth is required to produce good contrast fringe images. That is, a 24-bit color image can only encode three fringe images, thus the maximum fringe projection speed is limited by the digital video projector's maximum projection speed (typically 120 Hz).

Fundamentally, the first two limitations are essentially induced by the phase unwrapping of a single-wavelength phase-shifting technique. The phase unwrapping assumes that the phase changes between two neighboring pixel is not beyond π, thus any unknown changes or changes beyond cannot be correctly recovered. This hurtle can be overcome by using multiple-wavelength fringe images. For example, a digital multiple-wavelength technique can be adopted to solve this problem (Zhang, 2009). Using a multiple-wavelength technique will reduce the measurement speed significantly because more fringe images are required to perform one measurement. It has been indicated that at least three wavelength fringe images are required to measure arbitrary 3-D surfaces with arbitrary step heights (Towers et al., 2003). The speed is essentially limited by hardware, and is difficult to overcome for if the traditional method is used, where the grayscale fringe images has to be adopted. The image switching speed is essentially limited by the data sent to the projection system and the generation of the sinusoidal patterns. Recently, Lei & Zhang (2009) proposed a promising technology that realized a sinusoidal phase-shifting algorithm using binary patterns through projector defocusing. This technique may lead a breakthrough in this field because switching binary structured images can be realized in a much faster manner allowed by hardware.
Besides the speed and range challenges of the current real-time 3-D shape measurement techniques, there are a number of more challenging problems to tackle. The major challenges are:

1. *Shiny surfaces measurement*. Shiny surfaces are very common in manufacturing, especially before any surface treatment. How to measure this type of parts using the real-time 3-D shape measurement technique remains challenging. There are some techniques proposed (Chen et al., 2008; Hu et al., 2005; Zhang & Yau, 2009), but none of them are suitable for real-time 3-D measurement cases.

2. *Accuracy improvement*. The accuracy of the current real-time 3-D shape measurement system is not high. Part of the error is caused by motion of the object. This is because that the object is assumed to be motionless when the measurement is performed. However, to measure the object in motion, this assumption might cause problem. To meet the requirement in manufacturing engineering, it is very important to improve its system accuracy. One of the critical issues is the lack of standard for real-time 3-D shape measurement. Therefore, build a higher accuracy real-time 3-D shape measurement as a standard is very essential, but challenging.

3. *High-quality color texture measurement*. Although irrelevant to metrology, it is highly important to simultaneously acquire the high quality color texture, the photograph of the object, for numerous applications including computer graphics, medical sciences, and homeland security. For instance, in medical sciences, the 2-D color texture may convey critical information for diagnosis. We have developed a simultaneous color texture acquisition technique (Zhang & Yau, 2008). However, the object is illuminated by directional light (the projector's light). This is not desirable for many applications that requires very high quality 2-D color textures, where the object must be illuminated

with diffuse light uniformly. How to capture 3-D geometry and the color texture in real time and simultaneously becomes challenging.

6. Summary

We have covered the high-speed 3-D shape measurement techniques, especially focused on the system that was developed by our research group. The technology itself has numerous applications already. We have also addressed the limitations of the technology and the challenging questions we need to answer before this technology can be widely adopted.

7. Acknowledgements

First of all, I would like to thank this book editor, Dr. Vedran Kordic, for his invitation. My thanks also goes to my former advisors, Prof. Peisen Huang at Stony Brook University, and Prof. Shing-Tung Yau at Harvard University for their supervision. Some of the work was conducted under their support. I thank my students, Nikolaus Karpinsky, Shuangyan Lei, William Lohry, Ying Xu, and Victor Emmanuel Villagomez at Iowa State University for their brilliant work. Finally, I would like to thank my wife, Xiaomei Hao, for her consistent encouragement and support.

8. References

Baldi, A. (2003). Phase unwrapping by region growing, *Appl. Opt.* **42**: 2498–2505.

Blanz, V., Basso, C., Poggio, T. & Vetter, T. (2003). Reanimating faces in images and video, *Eurographics*, pp. 641–650.

Bleicher, J. N., Hamiel, S. & Gengler, J. S. (1996). A survey of facial paralysis: etiology and incidence, *Ear Nose Throat J.* **76**(6): 355–57.

Bowyer, K. W., Chang, K. & Flynn, P. J. (2006). A survey of approaches and challenges in 3d and multi-modal 3d+2d face recognition, *Comp. Vis. and Imag. Understand.* **12**: 1–15.

Bronstein, A. M., Bronstein, M. M. & Kimmel, R. (2005). Three-dimensional face recognition, *Intl J. of Comp. Vis. (IJCV)* **64**: 5–30.

Chen, Y., He, Y. & Hu, E. (2008). Phase deviation analysis and phase retrieval for partial intensity saturation in phase-shifting projected fringe profilometry, *Opt. Comm.* **281**(11): 3087–3090.

Cuevas, F. J., Servin, M. & Rodriguez-Vera, R. (1999). Depth object recovery using radial basis functions, *Opt. Commun.* **163**(4): 270–277.

Dhond, U. & Aggarwal, J. (1989). Structure from stereo-a review, *IEEE Trans. Systems, Man, and Cybernetics* **19**: 1489–1510.

Flynn, T. J. (1997). Two-dimensional phase unwrapping with minimum weighted discontinuity, *J. Opt. Soc. Am. A* **14**: 2692–2701.

Frey, M., Giovanolli, P., Gerber, H., Slameczka, M. & Stussi, E. (1999). Three-dimensional video analysis of facial movements: a new method to assess the quantity and quality of the smile, *Plast Reconstr Surg.* **104**: 2032–2039.

Gao, W., Wang, L. & Hu, Z. (2008). Flexible method for structured light system calibration, *Opt. Eng.* **47**(8): 083602.

Geng, Z. J. (1996). Rainbow 3-d camera: New concept of high-speed three vision system, *Opt. Eng.* **35**: 376–383.

Ghiglia, D. C. & Pritt, M. D. (eds) (1998). *Two-Dimensional Phase Unwrapping: Theory, Algorithms, and Software*, John Wiley and Sons, New York.

Ghiglia, D. C. & Romero, L. A. (1996). Minimum l^p-norm two-dimensional phase unwrapping, *J. Opt. Soc. Am. A* **13**: 1–15.

Guenter, B., Grimm, C., Wood, D., Malvar, H. & Pighin, F. (1998). Making faces, *SIGGRAPH*, pp. 55–66.

Guo, H. & Huang, P. (2008). 3-d shape measurement by use of a modified fourier transform method, *Proc. SPIE*, Vol. 7066, p. 70660E.

Guo, H. & Huang, P. S. (2009). Absolute phase retrieval for 3d shape measurement by fourier transform method, *Opt. Eng.* **48**: 043609.

Hadlock, T. A. & Cheney, M. L. (2008). Facial reanimation: an invited review and commentary, *Arch Facial Plast Surg.* **10**: 413–417.

Hadlock, T. A., Greenfield, L. J., Wernick-Robinson, M. & Cheney, M. L. (2006). Multimodality approach to management of the paralyzed face, *Laryngoscope* **116**: 1385–1389.

Hall-Holt, O. & Rusinkiewicz, S. (2001). Stripe boundary codes for real-time structured-light range scanning of moving objects, *The 8th IEEE International Conference on Computer Vision*, pp. II: 359–366.

Harding, K. G. (1988). Color encoded morié contouring, *Proc. SPIE*, Vol. 1005, pp. 169–178.

Heseltine, T., Pears, N. & Austin, J. (2008). Three-dimensional face recognition using combinations of surface feature map subspace components, *Image and Vision Computing (IVC)* **26**: 382–396.

Hu, Q., Harding, K. G., Du, X. & Hamilton, D. (2005). Shiny parts measurement using color separation, *SPIE Proc.*, Vol. 6000, pp. 6000D1–8.

Hu, Q., Huang, P. S., Fu, Q. & Chiang, F. P. (2003). Calibration of a 3-d shape measurement system, *Opt. Eng.* **42**(2): 487–493.

Huang, P. & Han, X. (2006). On improving the accuracy of structured light systems, *Proc. SPIE*, Vol. 6382, p. 63820H.

Huang, P. S., Hu, Q., Jin, F. & Chiang, F. P. (1999). Color-encoded digital fringe projection technique for high-speed three-dimensional surface contouring, *Opt. Eng.* **38**: 1065–1071.

Huang, P. S., Zhang, C. & Chiang, F.-P. (2002). High-speed 3-d shape measurement based on digital fringe projection, *Opt. Eng.* **42**(1): 163–168.

Huang, P. S. & Zhang, S. (2006). Fast three-step phase shifting algorithm, *Appl. Opt.* **45**(21): 5086–5091.

Huang, P. S., Zhang, S. & Chiang, F.-P. (2005). Trapezoidal phase-shifting method for three-dimensional shape measurement, *Opt. Eng.* **44**(12): 123601.

Huang, X., Zhang, S., Wang, Y., Metaxas, D. & Samaras, D. (2004). A hierarchical framework for high resolution facial expression tracking, *IEEE Computer Vision and Pattern Recognition Workshop*, Vol. 01, p. 22.

Huntley, J. M. (1989). Noise-immune phase unwrapping algorithm, *Appl. Opt.* **28**: 3268–3270.

Jia, P., Kofman, J. & English, C. (2007). Two-step triangular-pattern phase-shifting method for three-dimensional object-shape measurement, *Opt. Eng.* **46**(8): 083201.

Kakadiaris, I. A., Passalis, G., Toderici, G., Murtuza, N., Karampatziakis, N. & Theoharis, T. (2007). 3d face recognition in the presence of facial expressions: an annotated deformable model approach, *IEEE Trans. on Patt. Anal. and Mach. Intellig. (PAMI)* **29**: 640–649.

Kalberer, G. A. & Gool, L. V. (2002). Realistic face animation for speech, *Intl Journal of Visualization Computer Animation* **13**(2): 97–106.

Khailany, B., Dally, W., Rixner, S., Kapasi, U., Owens, J. & Towles, B. (2003). Exploring the vlsi scalability of stream processors, *Proc. 9th Symp. on High Perf. Comp. Arch.*, pp. 153–164.

Kim, S., Pakzad, S., Culler, D., Demmel, J., Fenves, G., Glaser, S. & Turon, M. (2007). Health monitoring of civil infrastructurtes using wireless sensor network, *Proc. 6th intl conference on information processing in sensor networks*, pp. 254–263.

Legarda-Sáenz, R., Bothe, T. & Jüptner, W. P. (2004). Accurate procedure for the calibration of a structured light system, *Opt. Eng.* **43**(2): 464Ű–471.

Lei, S. & Zhang, S. (2009). Flexible 3-d shape measurement using projector defocusing, *Opt. Lett.* **34**(20): 3080–3082.

Li, Z., Shi, Y., Wang, C. & Wang, Y. (2008). Accurate calibration method for a structured light system, *Opt. Eng.* **47**(5): 053604.

Linstrom, C. J. (2002). Objective facial motion analysis in patients with facial nerve dysfunction, *Laryngoscope* **112**: 1129–1147.

Lohry, W., Xu, Y. & Zhang, S. (2009). Optimum checkerboard selection for accurate structured light system calibration, *Proc. SPIE*, Vol. 7432, p. 743202.

Mehta, R. P., Zhang, S. & Hadlock, T. A. (2008). Novel 3-d video for quantification of facial movement, *Otolaryngol Head Neck Surg.* **138**(4): 468–472.

Pan, J., Huang, P. S. & Chiang, F.-P. (2005). Accurate calibration method for a structured light system, *Opt. Eng.* **44**(2): 023606.

Pan, J., Huang, P., Zhang, S. & Chiang, F.-P. (2004). Color n-ary gray code for 3-d shape measurement, *12th Intl Conf. on Exp. Mech.*

Queirolo, C. C., Silva, L., Bellon, O. R. & Segundo, M. P. (2009). 3d face recognition using simulated annealing and the surface interpenetration measure, *IEEE Trans. on Patt. Anal. and Mach. Intellig. (PAMI)* . doi:10.1109/TPAMI.2009.14.

Rusinkiewicz, S., Hall-Holt, O. & Levoy, M. (2002). Real-time 3d model acquisition, *ACM Trans. Graph.* **21**(3): 438–446.

Salvi, J., Pages, J. & Batlle, J. (2004). Pattern codification strategies in structured light systems, *Patt. Recogn.* **37**: 827–849.

Schreiber, H. & Bruning, J. H. (2007). *Optical Shop Testing*, 3rd edn, John Wiley & Sons, chapter Phase shifting interferometry, pp. 547–655.

Staszewski, W.J., L. B. C. T. R. (2007). Fatigue crack detection in metallic structures with lamb waves and 3d laser vibrometry, *Meas. Sci. Tech.* **18**: 727–729.

Stewart, B. M., Hager, J. C., Ekman, P. & Sejnowski, T. J. (1999). Measuring facial expressions by computer image analysis, *Psychophysiology* **36**: 253–263.

Su, X. & Zhang, Q. (2009). Dynamic 3-d shape measurement method: A review, *Opt. Laser. Eng* . doi:10.1016/j.optlaseng.2009.03.012.

Takeda, M. & Mutoh, K. (1983). Fourier transform profilometry for the automatic measurement of 3-d object shape, *Appl. Opt.* **22**: 3977–3982.

Tomat, L. R. & Manktelow, R. T. (2005). Evaluation of a new measurement tool for facial paralysis reconstruction, *Plast Reconstr Surg.* **115**: 696–704.

Towers, D. P., Jones, J. D. C. & Towers, C. E. (2003). Optimum frequency selection in multi-frequency interferometry, *Opt. Lett.* **28**: 1–3.

Ujaldon, M. & Saltz, J. (2005). Exploiting parallelism on irregular applications using the gpu, *Intl. Conf. on Paral. Comp.*, pp. 13–16.

Wang, Y., Gupta, M., Zhang, S., Wang, S., Gu, X., Samaras, D. & Huang, P. (2008). High resolution tracking of non-rigid 3d motion of densely sampled data using harmonic maps, *Intl J. Comp. Vis.* **76**(3): 283–300.

Wang, Y., Huang, X., Lee, C.-S., Zhang, S., Li, Z., Samaras, D., Metaxas, D., Elgammal, A. & Huang, P. (2004). High-resolution acquisition, learning and transfer dynamic 3d facial expression, *Comp. Graph. Forum* **23**(3): 677 – 686.

Yang, R., Cheng, S. & Chen, Y. (2008). Flexible and accurate implementation of a binocular structured light system, *Opt. Lasers Eng.* **46**(5): 373–379.

Zhang, S. (2009). Digital multiple-wavelength phase-shifting algorithm, *Proc. SPIE*, Vol. 7432, p. 74320N.

Zhang, S. (2010). Recent progresses on real-time 3-d shape measurement using digital fringe projection techniques, *Opt. Laser Eng* **40**: 149–158.

Zhang, S. & Huang, P. (2004). High-resolution, real-time 3-d shape acquisition, *IEEE Comp. Vis. and Patt. Recogn. Workshop*, Vol. 3, Washington DC, MD, pp. 28–37.

Zhang, S. & Huang, P. S. (2006a). High-resolution, real-time three-dimensional shape measurement, *Opt. Eng.* **45**(12): 123601.

Zhang, S. & Huang, P. S. (2006b). Novel method for structured light system calibration, *Opt. Eng.* **45**: 083601.

Zhang, S., Li, X. & Yau, S.-T. (2007). Multilevel quality-guided phase unwrapping algorithm for real-time three-dimensional shape reconstruction, *Appl. Opt.* **46**(1): 50–57. (Selected for February 5, 2007 issue of The *Virtual Journal for Biomedical Optics*).

Zhang, S., Royer, D. & Yau, S.-T. (2006). Gpu-assisted high-resolution, real-time 3-d shape measurement, *Opt. Express* **14**: 9120–9129.

Zhang, S. & Yau, S.-T. (2007). High-speed three-dimensional shape measurement using a modified two-plus-one phase-shifting algorithm, *Opt. Eng.* **46**(11): 113603.

Zhang, S. & Yau, S.-T. (2008). Simultaneous three-dimensional geometry and color texture acquisition using single color camera, *Opt. Eng.* **47**(12): 123604.

Zhang, S. & Yau, S.-T. (2009). High dynamic range scanning technique, *Opt. Eng.* **48**: 033604.

Zhang, Z. (2000). A flexible new technique for camera calibration, *IEEE Trans. Pattern Anal. Mach. Intell.* **22**(11): 1330–1334.

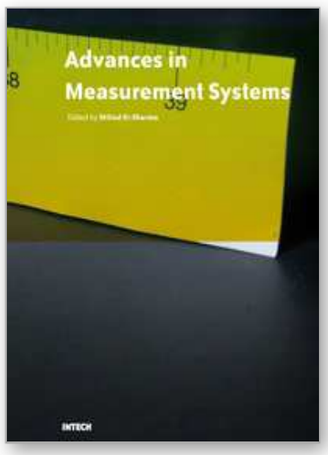

Advances in Measurement Systems

Edited by Milind Kr Sharma

ISBN 978-953-307-061-2
Hard cover, 592 pages
Publisher InTech
Published online 01, April, 2010
Published in print edition April, 2010

How to reference

In order to correctly reference this scholarly work, feel free to copy and paste the following:

Song Zhang (2010). High-resolution, High-speed 3-D Dynamically Deformable Shape Measurement Using Digital Fringe Projection Techniques, Advances in Measurement Systems, Milind Kr Sharma (Ed.), ISBN: 978-953-307-061-2, InTech, Available from: http://www.intechopen.com/books/advances-in-measurement-systems/high-resolution-high-speed-3-d-dynamically-deformable-shape-measurement-using-digital-fringe-project

INTECH
open science | open minds

InTech Europe
University Campus STeP Ri
Slavka Krautzeka 83/A
51000 Rijeka, Croatia
Phone: +385 (51) 770 447
Fax: +385 (51) 686 166
www.intechopen.com

InTech China
Unit 405, Office Block, Hotel Equatorial Shanghai
No.65, Yan An Road (West), Shanghai, 200040, China
中国上海市延安西路65号上海国际贵都大饭店办公楼405单元
Phone: +86-21-62489820
Fax: +86-21-62489821

IntechOpen